Mechanical behavior of 3D printed polymers under tensile and bending loads

Alberto Saldaña-Robles[1], Alexis Sánchez-Angeles[2], Antonio de J. Balvantín-García[2],
Diego A. Núñez-Altamirano[2], Gustavo Capilla-González[2*]

[1] Agricultural Engineering Department, Life Sciences Division, University of Guanajuato, 36500, Irapuato, Guanajuato, Mexico
[2] Mechanical Engineering Department, Engineering Division, University of Guanajuato, 36885, Salamanca, Guanajuato, Mexico
* Corresponding author's e-mail: g.capilla@ugto.mx

ABSTRACT

This study investigates the effects of infill orientation, infill density, and printing speed on the mechanical behavior of PLA, ABS, and PETG materials. Using Taguchi's DoE approach, relevant mechanical properties determined from uniaxial tensile and four-point bending tests were statistically analyzed to assess their significance. Results indicate that infill orientation and infill density significantly influence the mechanical properties of the materials, whereas printing speed showed minimal impact. The stress-strain for the three materials determined from uniaxial are presented. Furthermore, 3D surfaces plots describing the interaction between the parameters are presented and discussed. These findings provide systematized and accessible information for optimizing 3D printing parameters and calibrating finite element models to predict the behavior of printed components under tensile and bending loads.

Keywords: additive manufacturing, 3D printing, FDM, mechanical properties.

INTRODUCTION

Additive Manufacturing (AM) has emerged as a robust technology for prototyping across various sectors, offering significant reductions in cost and manufacturing time. It enables the creation of complex structures through layer-by-layer material deposition using digitally controlled tools, ensuring high precision and minimal material waste. [1, 2]. Also, on-demand and customized products will significantly reduce the need for assembly operations and inventory, leading to a quicker transfer to the final consumer [3]. Industries such as automotive [4], aerospace, and medical [5, 6] have embraced AM prototyping and product development technologies. Among the various techniques in AM, methods like fusion deposition modeling (FDM) have emerged as particularly relevant due to their flexibility and low cost of thermoplastic materials such as polylactic acid (PLA),

acrylonitrile butadiene styrene (ABS), and polyethylene terephthalate (PETG). According to Carneiro et al. [7], FDM is showing excellent prospects for product development with the ability to compete against conventional polymer processing techniques such as plastic injection. In the forecast presented in the Market Research Report, the global additive manufacturing market will grow exponentially in the coming years, from USD 453.3 million in 2020 to USD 1,496.7 million in 2028. However, the success of adopting the AM as a technology for the manufacture of commercial components relies on the performance of the parts during the on-serving life cycle, compliance with the established standards, and assurance of the mechanical and physical material properties. Furthermore, the production cost must be competitive with the current manufacturing processes. To fulfill this purpose, analyzing the influence of the printing parameters on the mechanical properties

of thermoplastic materials under several load conditions is vital to knowing the capabilities of the printed products.

During the last decade, several authors have focused on investigating the mechanical behavior of 3D-printed materials. Cojocaru et al. [8] presented a detailed review of process parameters that influence the strength of the PLA under the uniaxial tensile test showing that the ultimate tensile strength (UTS) is slightly affected by the layer thickness and printing speed, pointing out that a high material flow rate reduces the solidification time, promoting the adhesion mechanism between layers. Akhoundi and Behravesh [9] analyzed the effect of infill patterns and densities on tensile strength, flexural strength, and elasticity modulus in PLA specimens. The results showed that the higher strength under tensile and flexural loads was obtained using a concentric infill pattern. Also, short printing paths help to maintain a stable temperature, contributing to the bonding of the adjacent filaments and increasing the strength resistance of the material. Travieso et al. [10] conducted an experimental study employing bending and fatigue tests in PLA specimens. A design of experiments (DoE) based on Taguchi's formulation with six parameters and three levels was implemented. The statistical analysis of the bending tests shows that the layer orientation, layer height, and filament width strongly influence the Young modulus, yield strength, and ultimate strength. Cantrell et al. [11] evaluated the anisotropy of FDM-printed ABS specimens by uniaxial and shear tests. Raster orientations of [+45/-45], [+30/-60], [+15/-75], [0/90], and build orientations on in-plane, edge, and up-right were analyzed. Uniaxial tensile results show that an in-plane specimen's strain energy density can be 91% higher than up-right specimens for the same raster orientation. Samykano et al. [12] show the uniaxial tensile results of ABS specimens considering three raster angles (0°, 45°, and 90°), three infill densities (40, 60, and 80%), and three-layer heights (0.35, 0.4 and 0.5 mm). Reported results show that the increase in the infill density is directly related to the material strength expressed in terms of the Young modulus and UTS. Sepahi et al. [13] analyzed the mechanical properties of uniaxial tensile in PLA, ABS, and PETG specimens using different raster angles. In summary of the work, PETG offers a better elongation to break than PLA and ABS materials. Also, it is reported that the fracture type (brittle or ductile) depends on the raster orientation in the specimens. This fact was demonstrated through SEM micrographs of the specimens. Khan et al. [14] tested uniaxial and bending specimens printed with rectilinear, concentric, honey-comb, and Hilbert curve patterns. Reported results showed that the rectilinear pattern increased the Young modulus to 10.51 GPa and tensile strength up to 19.1 MPa. Shubham et al. [15] analyzed the influence of layer thickness on printed and molded injected tensile samples. Four-layer thicknesses of 0.075, 0.1, 0.25, and 0.5 mm were studied. Experimental results showed that injected samples exhibited higher tensile, impact strength, and hardness. For the 3D printed samples, it was found that increasing the thickness layer affects the mechanical behavior of samples. Based on Taguchi's model, Valvez et al. [16] conducted a statistical analysis to evaluate the effect of nozzle temperature, printing speed, layer height, and filling in fabricated PETG and PETG+CF (carbon fiber) specimens. Results showed that higher strength values were attained for samples with thinner layers. This is because thicker layers overlapping the previous ones have already solidified, which does not guarantee a good adhesion between them. Thus, the analysis must include nozzle temperature to optimize solidification and adhesion conditions. Also, in recent works, authors have devoted their efforts to analyzing new composite filaments [17–20], thermal processes [21–24], and surface finishing processes [25] to enhance the mechanical performance of the materials. Rahmatabadi et al. [26] conducted a complete experimental study to determine the mechanical properties under tension, compression, bending, shear, and fracture tests. The specimens were fabricated by using a PLA-TPU compound matrix at different temperatures. The results showed that TPU (Thermoplastic Polyuretane) added flexibility to the matrix while PLA effectively increased its strength. Chueca et al. [27] investigated the effect of the ball burnishing process as a surface plastic deformation method on the tensile, flexural, flexural fatigue and impact mechanical properties of a PEI thermoplastic. Following Taguchi's model, the experiments showed that burnishing force and number of passes are the most significant parameters for improving surface quality. Also, the hardness of the material substantially increased concerning the raw material.

Furthermore, authors have been focused on the use of material parameters for the calibration of finite element (FE) models, to predict its

response under several loading conditions. Perera et al. [28] used the FE simulation as a virtual machine to determine the optimal mechanical properties of hollow structures before printing. The study was conducted using tensile and bending tests in ABS and PLA materials. Results confirmed that the FE models were able to predict the tensile and bending behavior in a plastic deformation range. However, the failure of the materials was underestimated. Abbot et al. [29] evaluated the density and infill orientation of compression specimens fabricated from TPU, PETG, and PLA materials by FDM process. From the experimental and numerical results, it is concluded that advanced numerical models are necessary to represent the effect of voids between layers generated in the printing process. Alarifi [30] evaluated the mechanical properties of four types of cellular structure (solid, circle, hexagonal auxetic, and reentrant) by uniaxial tensile test. Specimens of PETG/CF were fabricated using FDM. FE analyses were conducted to evaluate the mechanical response of a structural component constructed with the proposed cellular structures. Results show that reentrant structure can be customized to redistribute the flexural stress in components. Also, FE modeling allowed to demonstrate the exceptional bending resistance of auxetic panels; making them suitable for energy absorption applications. Alharbi et al. [31] reproduced the uniaxial stress-strain response of a PLA tensile specimen using a nonlinear analysis. Mechanical properties such as Young´s modulus, Poisson ratio, yield strength, and ultimate stress were used to calibrate the FE model, guaranteeing a maximum difference of 6.7% between the numerical and experimental results. Savik et al. [32] used a combined approach to evaluate the fracture resistance of PLA specimens under uniaxial loading. To capture the strain field, an advanced digital image correlation (DIC) system was used. The FE model with a brittle fracture criterion governed by the Hashing damage model was implemented. Results show that FE simulation reproduces in good agreement the experiments in different raster angles (0°, 45°, 90°). However, further studies are necessary for different materials. Provaggi et al. [33] used FE analysis to evaluate the mechanical performance of a lumbar fusion cage. Experimentally, the influence of the infill pattern, infill density, and type of material were evaluated. FE results show that honeycomb structures exhibited higher compressive properties and dimensional accuracy than rectangular patterns.

Based on the reviewed information, due to the vast number of parameters that can be modified in the printing process, coupled with many manufacturers, there are no definitive conclusions on the effect of all the parameters on the mechanical performance of 3D printed components. Furthermore, the wide variety of raw printing materials increases the variability of mechanical parameters. Thus, this work aims to analyze and discuss the mechanical properties determined from uniaxial tensile and four-point bending tests in additive-manufactured specimens by including three of the most relevant printing parameters. The results obtained in this work will be helpful for identification of the best parameter combinations that enhance the mechanical performance of the analyzed materials. Also, these experimental results will be useful in future work considering finite element simulation as a key tool to evaluate the performance of 3D printed components.

EXPERIMENTAL PROCEDURES

Materials and specimens' manufacture

This experimental study assesses material behavior under uniaxial tensile and bending loads in PLA, ABS, and PETG. The ASTM D638 (Type 1) and ASTM D6272 standards defined the uniaxial tensile and bending specimen's geometries and test parameters, respectively. Due to the difference in the material composition and thermal properties of the printed materials, specific nozzles and beds temperatures were used for each material, as listed in Table 1.

The specimens were fabricated in a Anycubic KobraMax printer with $450 \times 400 \times 400$ mm of printing space. Filaments with 1.75 mm diameter from the brand Color Plus and a nozzle of 0.4 mm were used. Ultimaker cura software was used for the specimens preprocessing and G-code generation, considering a layer height of 0.15 mm, five top and bottom layers, 0.8 mm of wall thickness, a skirt build plate adhesion type and a lines infill pattern.

Taguchi experimental design

A design of experiments (DoE) based on the Taguchi L9 was considered for the tensile and four-point bending specimens to analyze the experimental results statistically. Three parameters and three levels that have a high impact on the

Table 1. Bed and nozzle temperatures for printing PLA, ABS and PETG

Material	Bed Temp (°C)	Nozzle Temp (°C)
PLA	60	200
ABS	80	240
PETG	70	240

mechanical behavior of the materials listed in Table 2, were considered. To ensure the repeatability of the experiments, each condition was assessed in triplicate.

Table 3 lists the nine experimental conditions (T1 to T9) generated by the factorial design for each material. These conditions vary from infill orientation, infill density, and printing speed, serving as the basis for mechanical testing.

Experimental setup for tensile and bending tests

Figure 1 a) shows the experimental setup of the uniaxial tensile test conducted in the universal testing machine Instron 8872, with a 25 kN load capacity. Hydraulic jaws with a clamping pressure of 100 psi were used, enough to hold the specimens without deformation in the clamping zone. A 50 mm gage length extensometer was used to measure the strain during the experiments (Figure 1 b). To consider the effect of the thinning related to the transverse deformation (ε_2) and through thickness deformation (ε_3) the instantaneous deformation ε (true strain) defined by the Equation 1, were considered.

$$\varepsilon = \int_{l_0}^{L} \frac{dL}{L} = \ln\left(\frac{L}{L_0}\right) = \ln\left(\frac{A}{A_0}\right) \tag{1}$$

where: L_0 and A_0 are the initial length and area, respectively, L and A are the final length and area, respectively.

Also, by assuming a constant volume through the incompressibility condition where $\varepsilon_1 + \varepsilon_2 + \varepsilon_3 = 0$, the stress considering the change in the cross-sectional area (true stress) is expressed in Equation 2:

$$\sigma_T = ln(1 + e) \tag{2}$$

where: e is the engineering strain.

A four-point bending tooling designed under the ASTM D6272 standard was adapted to the universal testing machine, as shown in Figure 2. The load was recorded using a load cell with a precision of 0.002% of the maximum load. Rectangular specimens of 104 mm in length, 16 mm in width, and 5 mm in thickness were fabricated and placed between two circular fixed supports with 80 mm span, as is illustrated in Figure 3. A rigid double-punch loaded the specimens with a constant crosshead speed of 2.368 mm/min, up to one of the following conditions takes place: i) a maximum longitudinal strain of 5% is reached, ii) fracture occurs in the specimen before 5% of longitudinal strain. Under pure bending load conditions, the maximum stress was localized at the midpoint of the specimens, corresponding to the region of maximum deflection. The deflection was quantified through a quadrangular grid positioned at the rear of the experimental apparatus.

RESULTS AND DISCUSSIONS

The following section presents a detailed analysis of the tensile and bending responses, emphasizing the impact of infill orientation and infill density on material performance.

Uniaxial tensile results

The uniaxial stress-strains curves determined for the nine T-combinations are presented in Figure 4, Figure 5, and Figure 6; for the PLA, ABS, and PETG, respectively.

It can be observed that the printing process influences the workhardening represented by the plastic part of the stress-strain curves. For the PLA, for the T1, T2 and T3 specimens (infill

Table 2. Parameters and levels used in the factorial DoE

Parameter	Level		
	1	2	3
Infill density [%]	50	75	100
Infill orientation [°]	0	45	90
Printing speed [mm/seg]	10	50	90

Table 3. Rectangular matrix based on Factorial Design

Set	Infill orientation [°]	Infill density [%]	Printing speed [mm/seg]
T1	0	50	10
T2	0	75	50
T3	0	100	90
T4	45	50	50
T5	45	75	90
T6	45	100	10
T7	90	50	90
T8	90	75	10
T9	90	100	50

orientation parallel to the loading axis), the material exhibits a sharp yield point in the elastic part followed by a stagnated plastic deformation zone, like an elastic-perfect plastic material. However, for the other printing orientations (diagonal and transverse), an almost linear elastic behavior is observed.

ABS samples printed in a parallel direction show a larger elastic zone and a significantly lower Young´s modulus compared to PLA material. However, a reduced plastic zone with a softening (opposite to workhardening) behavior is observed. On the other hand, for the diagonal and transverse directions, a not clear transition between the elastic and plastic zones is observed, and a reduced ultimate strain with values around $0.015 \leq \varepsilon_u \leq$ is exhibited.

Finally, the stress-strain curves of the PETG material show a linear elastic behavior with a brittle fracture appearance during the tests. However, the tensile strength values for PETG are notably higher than those of PLA and ABS under similar conditions, except for the T4 and T7 specimens. This superior performance can be attributed to enhanced interlayer bonding, as suggested by other studies reporting tensile strengths for PETG in the range of 30–50 MPa, significantly higher than typical values for PLA (20–40 MPa) and ABS (20–35 MPa) under comparable conditions [13, 15]. These results highlight PETG's potential for higher strength and stiffness applications, particularly in load-bearing components.

The mechanical properties determined from the uniaxial tensile test under each condition are listed in Table 4, Table 5, and Table 6 for the PLA, ABS, and PETG, respectively. In those tables: M – Material, E – Young modulus, Sy – Yield strength, Su – Ultimate strength, and ε_u – Ultimate strain.

To detect outliers from normality and guarantee the correct statistical behavior of the data, the Anderson-Darling (AD) test was used for the four variables. From all the data, only the values of the ultimate strain for PLA material did not accomplish the assumption of normality; hence, for this response, the natural log transformation was applied. The ANOVA results were analyzed with a 95% confidence level for E, Sy, Su, and ε_u for PLA, ABS, and PETG materials. If the p-value of
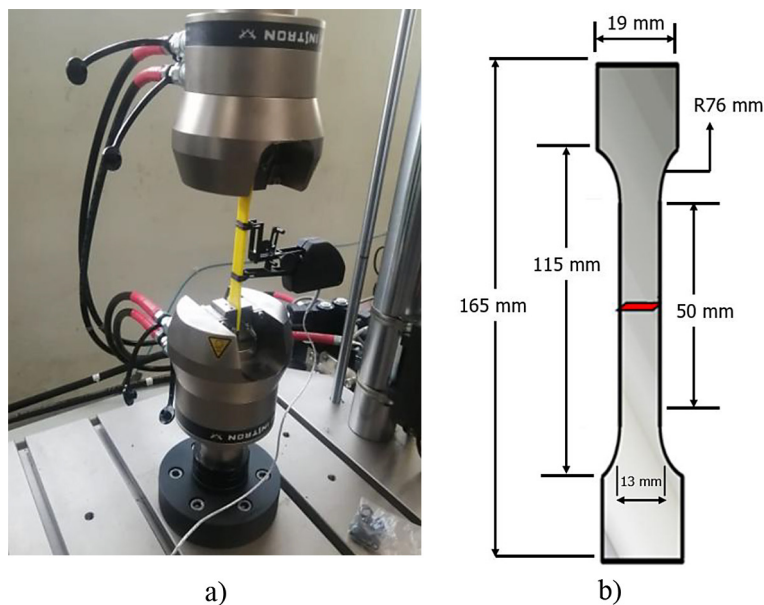

Figure 1. a) Experimental setup of the uniaxial tensile test according to the ASTM D638; b) Dimensions of the specimen
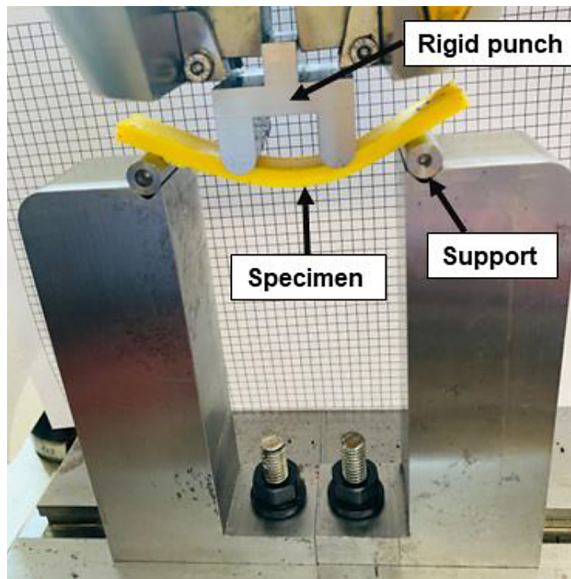
Figure 2. Experimental setup of the four-point bending test according to the ASTM D6272

the source is below 0.05, it shows the significance of the parameter. The percentage contribution of the parameters to each response obtained from the sum of squares was also calculated.

For the PLA material, the most significant factor influencing all responses in this study was the infill orientation, which aligns with findings in the literature [8]. Infill orientation had the greatest percentage contribution with 67.7%, 80.6%, 74.0%, and 93.9% for E, Sy, Su, and ε_u, respectively. Although infill density was not a significant parameter, it was the second parameter with the highest percentage contribution. Also, the printing speed was statistically significant for ε_u. Moreover, this parameter presented the lower contribution percentages, between 0.3% and 3.7%. These results emphasize the importance of

optimizing infill orientation for applications requiring high stiffness or strength.

In contrast to PLA, in ABS and PETG materials, the infill density was the parameter with the greatest percentage contribution over E, Sy, and Su responses, while for the ε_u, the response was the infill orientation. For both materials, ABS and PETG, the printing speed parameter was not significant in all responses (E, S_y, S_u, and εu), with p-values over 0.05. Also, the percentage contribution of the printing speed was low for all responses in both materials compared to the infill orientation and infill density, like PLA results. For ABS, the percentage contribution of printing speed was 0.7%, 0.4%, 1.3%, and 2.4% for E, Sy, Su, and εu, respectively, while for PETG, it was 9.2%, 2.9%, 1.8%, and 8.2% for the same responses. The results of this work suggest that the infill orientation and infill density contribute considerably to the change in mechanical properties E, Sy, Su, and εu, while the printing speed is not so relevant.

Figure 7 (a), (b), and (c) display the main effects plots for the yield strength (Sy) of PLA, ABS, and PETG materials, respectively. These plots reveal that infill orientation and infill density are the most influential parameters affecting Sy, with the highest contributions observed for both materials across all tested levels. Conversely, printing speed showed a negligible effect on Sy, consistent with its minimal contribution percentage. Similar trends were observed for other mechanical properties (E, S_u, and ε_u), confirming the dominant role of infill orientation and infill density. These findings underscore the significance of aligning infill orientation and optimizing infill density to enhance mechanical performance.
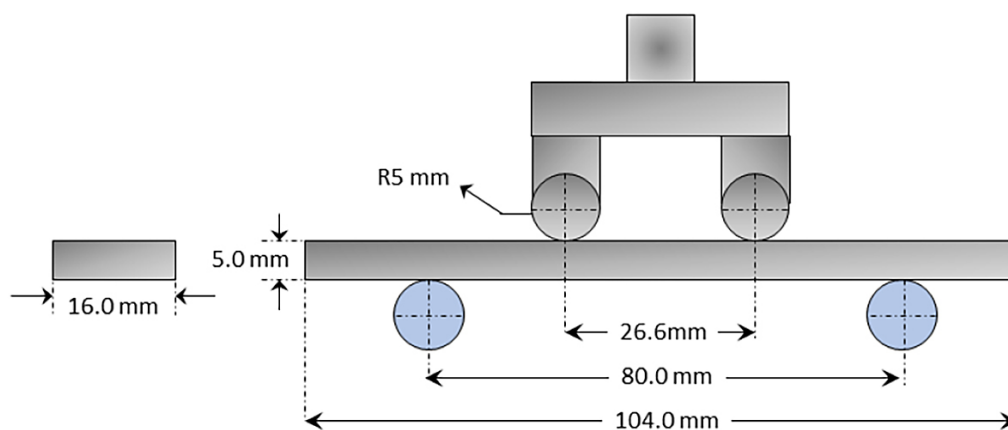

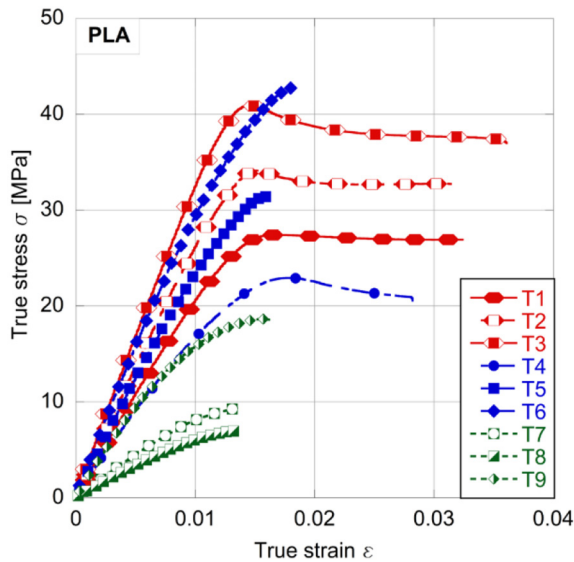**Figure 3.** Geometrical parameters of the four-point bending tool

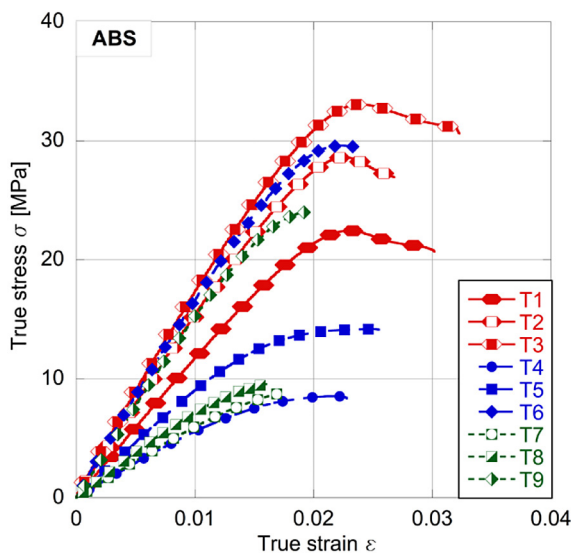**Figure 4.** True stress vs. true strain curves for the PLA material

Figure 5. True stress vs. true strain curves or the ABS material

Figure 8 presents 3D surface plots illustrating the influence of infill orientation and infill density on the mechanical properties (E, Sy, Su, and εu) derived from the uniaxial tensile test for PLA, ABS, and PETG materials. The printing speed parameter was fixed at its medium level (50 mm/s), given its low contribution to the overall responses. These surfaces were modeled using a linear regression approach, yielding correlation coefficients (R^2) ranging from 0.82 to 0.95. The high R^2 values indicate a strong fit of the linear models, making them suitable for analyzing the effects of input parameters on the measured mechanical properties.

Each surface graph was modeled using a linear model with correlation coefficients (R^2) between 0.82 and 0.95. Thus, these selected models were considered appropriate for analyzing the effect of the input parameters on the output responses.

Figure 8 a) presents the Young modulus (*E*) surface plot where PLA material exhibits the highest elastic modulus, followed by the PETG and the ABS. Across all materials, the Young's modulus decreases as the infill orientation changes from 0° to 90°, with a higher slope in the PLA material. The superior performance of PLA could be linked to its enhanced interlayer adhesion, which reduces void formation and promotes stronger bonding between layers. This behavior aligns with findings reported in the literature, where interlayer adhesion mechanisms are identified as key contributors to the mechanical performance of 3D-printed polymers [34].

Figure 8 b) shows the yield strength of the ABS, PLA, and PETG materials. The maximum values are obtained at a infill orientation of 0° with an infill density of 100%. By reducing the infill density (to 75% and 50%) and with diagonal and transverse infill orientation, the yield strength is significantly reduced for all materials. Also, diagonal and transverse-oriented specimens subjected to micrographic analysis exhibit a lack of adhesion in deposited layers, influencing material strength [35]. This work obtains minimum yield strength for specimens oriented in 90°.

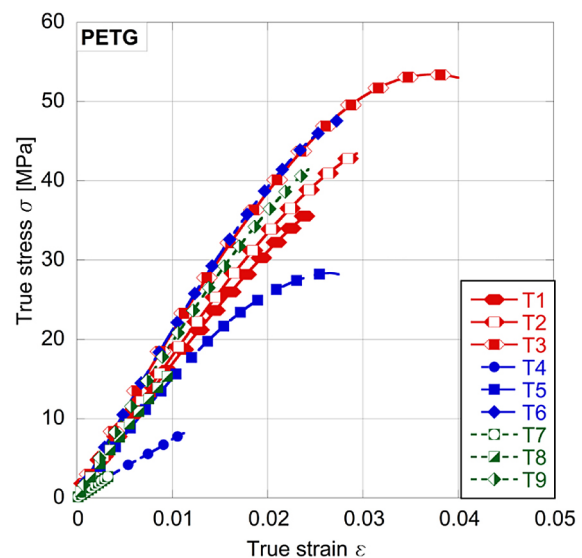Figure 8 c) shows the surface plot of the ultimate strength S_U of ABS, PLA, and PETG

Figure 6. True stress vs. true strain curves for the PETG material

Table 4. Experimental results of the uniaxial tensile test for the PLA material

Set	PLA			
	E [MPa]	[MPa]	S_u [MPa]	ε_u
T1	2306	28.83	27.44	0.03150
T2	2561	32.85	31.91	0.03200
T3	3221	39.73	37.46	0.03175
T4	1693	19.01	19.83	0.01960
T5	2383	26.75	27.26	0.01330
T6	3048	33.80	35.67	0.01795
T7	843	8.64	8.84	0.01270
T8	623	6.75	6.75	0.01320
T9	1767	15.28	18.48	0.01730

Table 5. Experimental results of the uniaxial tensile test for the ABS material

Set	ABS			
	E [MPa]	S_y [MPa]	S_u [MPa]	ε_u
T1	1164	20.87	21.54	0.03210
T2	1516	25.82	29.82	0.02595
T3	1689	29.84	32.54	0.02970
T4	577	7.68	9.49	0.02160
T5	1640	21.11	25.92	0.02180
T6	1752	27.68	29.28	0.02510
T7	574	8.36	8.36	0.01665
T8	741	9.32	9.32	0.01520
T9	1555	22.21	23.16	0.01890

Table 6. Experimental results of the uniaxial tensile test for the PETG material

Set	PETG			
	E [MPa]	S_y [MPa]	S_u [MPa]	ε_u
T1	1759	26.34	34.54	0.02420
T2	1777	31.40	41.56	0.02985
T3	2144	39.66	50.65	0.03320
T4	758	8.37	8.37	0.02300
T5	1640	21.11	25.92	0.02300
T6	2153	38.01	46.47	0.02675
T7	765	4.33	4.33	0.00600
T8	1610	15.71	15.71	0.00975
T9	2031	32.18	40.68	0.02400

materials. It is observed that PETG printed with infill oriented at 0° with 100% infill density provides remarkably higher strength, but for densities of 75 and 50%, ultimate strength is considerably reduced. A similar tendency is observed for the PLA and ABS specimens. Furthermore, specimens tested with infill orientated at 45° and 90° show a reduction in the ultimate strength. The weaker parameter combination is obtained for specimens printed at 90° with an infill density of 50%.

Finally, Figure 8 d) shows the ultimate strain ε_u results. It should be noted that infill orientation
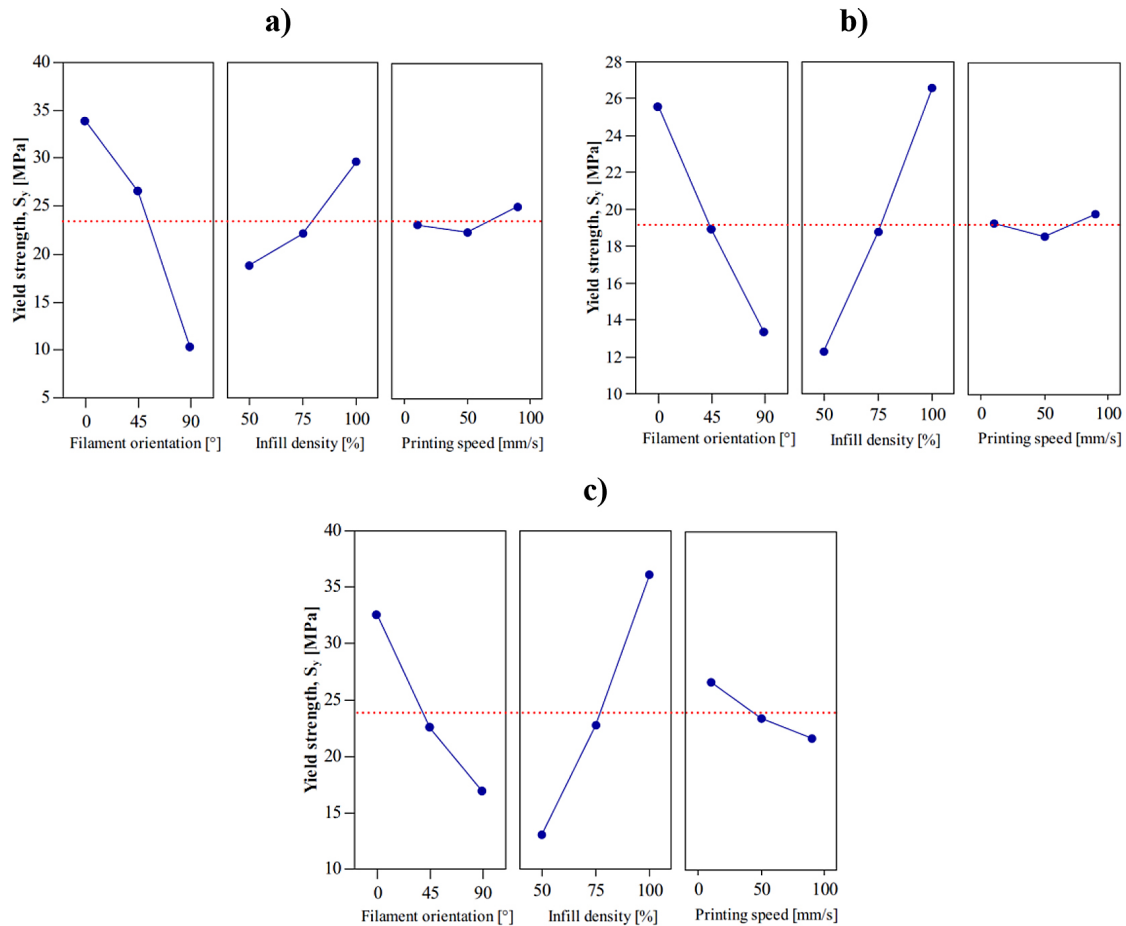
a)

b)

c)

Figure 7. Main effects plot for means of the yield strength (S_y) for: (a) PLA, (b) ABS and (c) PETG materials

and infill density play a crucial role in the magnitude of this parameter. The maximum ε_u values were obtained for the 0° with a 100% infill density. On the other hand, 90°, with a 50% infill density, shows the lower values.

Four-point bending results

The experimental results of the four-point bending test expressed in terms of the maximum bending stress σ_b and the maximum bending strain ε_b are listed in Table 7, Table 8, and Table 9 for the three materials.

ANOVA results with a 95% confidence level were conducted for mechanical properties of bending – maximum bending stress (σ_b) and maximum bending strain (ε_b) – for PLA, ABS, and PETG materials. Like the mechanical properties determined from the uniaxial tensile test, the infill orientation and infill density parameters show the highest contribution percentages for the mechanical properties obtained from the bending test (σ_b and ε_b). In addition, the printing speed parameter

was not statistically significant over σ_b and ε_b according to the levels studied in this work. Also, the printing speed parameter presented the lowest percentage contributions compared to the other parameters studied.

The main effects plots for means of maximum bending stress (σb) for the three materials studied are presented in Figure 9. The strong contribution of the infill orientation and infill density in the maximum bending stress (σb), likewise it is observed that the lowest contribution is provided by the printing speed parameter. Similar results were obtained for maximum bending strain (εb) response. Similar findings of the analyzed parameters were reported by Travieso et al. for a PLA material [10].

Finally, the 3D surface graphs of the effect of infill orientation and infill density for maximum bending stress (σ_b) and maximum bending strain (ε_b) are shown in Figure 10. These plots are presented for printing speed with a medium level of 50 mm/s and the linear models obtained have correlation coefficients (R^2) from 0.82 to 0.94.
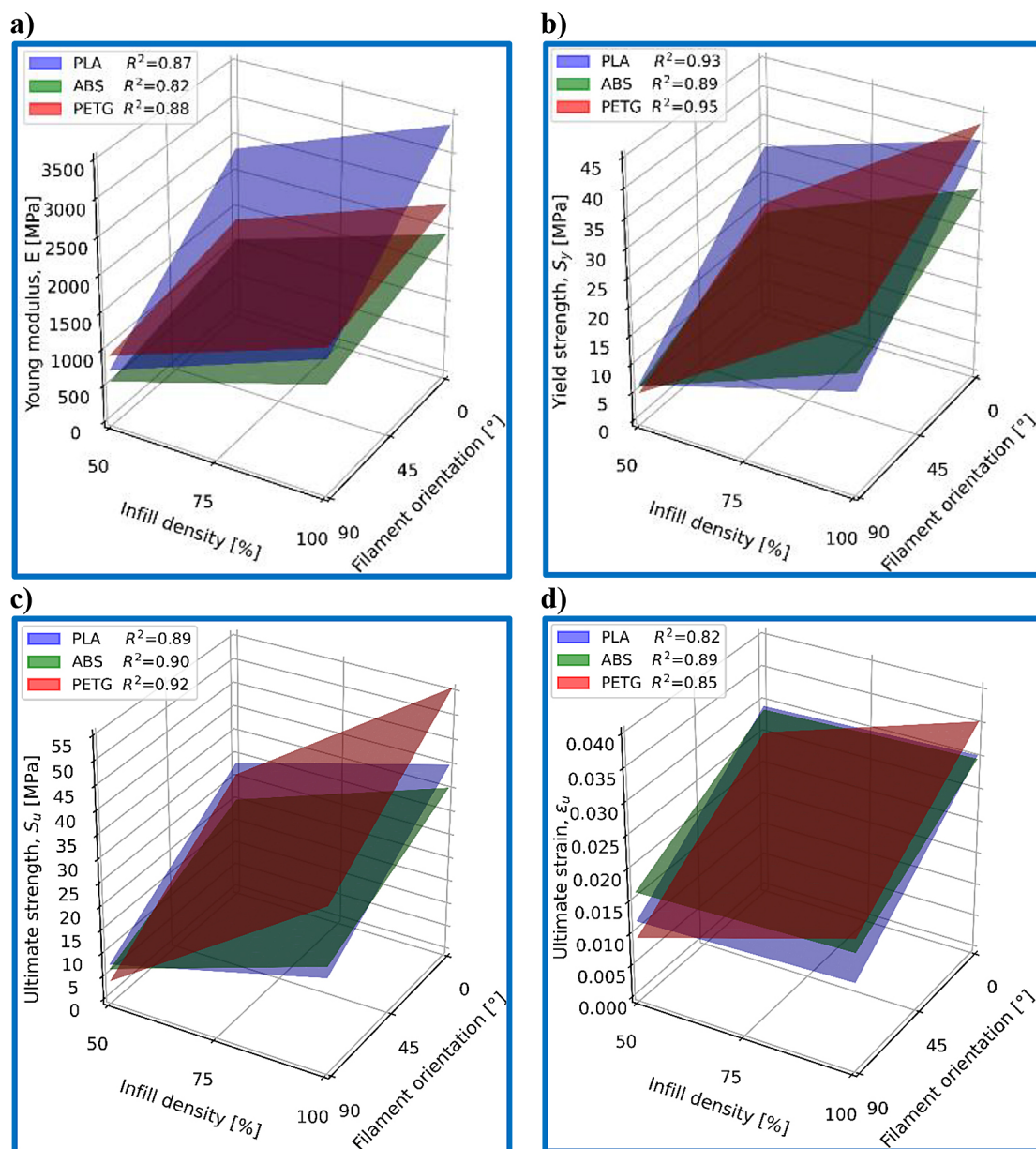
Figure 8. Surface plots for the mechanical properties of the uniaxial tensile test for PLA, ABS and PETG materials, (a) Young modulus (E), (b), yield strength (S_y) (c) ultimate strength (S_u) and (d) ultimate strain (ε_u)

Table 7. Experimental results of the four-point bending results for the PLA material

Material	PLA	
Set	σ_b [MPa]	ε_b
T1	48.72	0.061
T2	54.48	0.078
T3	60.28	0.113
T4	42.44	0.048
T5	37.52	0.079
T6	62.52	0.089
T7	11.87	0.037
T8	17.94	0.045
T9	28.72	0.043

Table 8. Experimental results of the four-point bending results for the ABS material

Material	ABS	
Set	σ_b [MPa]	ε_b
T1	41.78	0.078
T2	49.44	0.099
T3	55.30	0.108
T4	36.55	0.045
T5	45.76	0.084
T6	50.97	0.092
T7	10.66	0.046
T8	18.48	0.076
T9	45.01	0.066

Table 9. Experimental results of the four-point bending results for the PETG material

Material	PETG	
Set	σ_b [MPa]	ε_b
T1	42.02	0.040
T2	51.79	0.068
T3	54.39	0.113
T4	30.46	0.048
T5	26.48	0.079
T6	51.73	0.089
T7	11.79	0.034
T8	14.83	0.054
T9	28.40	0.074

Figure 10 a) presents the bending stress results where it can be observed that the three materials' behaviors are described by plane surfaces with similar trends showing their maximum value for samples with 100% infill density and filament direction of 45° in the case of PLA and 0° for the ABS and PETG. This is expected because, as is well known, specimens under pure bending loads experience almost uniaxial tensile and compressive stress states on the bottom and upper surfaces, respectively. Thus, filaments aligned with the normal stress direction will increase the strength of the material, showing its maximum value. On the other hand, minimum bending stresses are obtained for the lower infill density of 50% and 90° orientation.

Figure 10 b) shows the surface plot of the maximum bending strain regarding the infill density and infill orientation. It can be observed that the lineal model accurately describes the experimental behavior of the three materials. Maximum bending stress and maximum bending strain are obtained with 0° infill orientation and 100% infill density. On the other hand, minimum bending strains were obtained with 90° infill orientation and 50% infill density for the PLA and PETG, respectively. In the case of the ABS material, the minimum was obtained with an infill density of 50% and 45° of infill orientation.
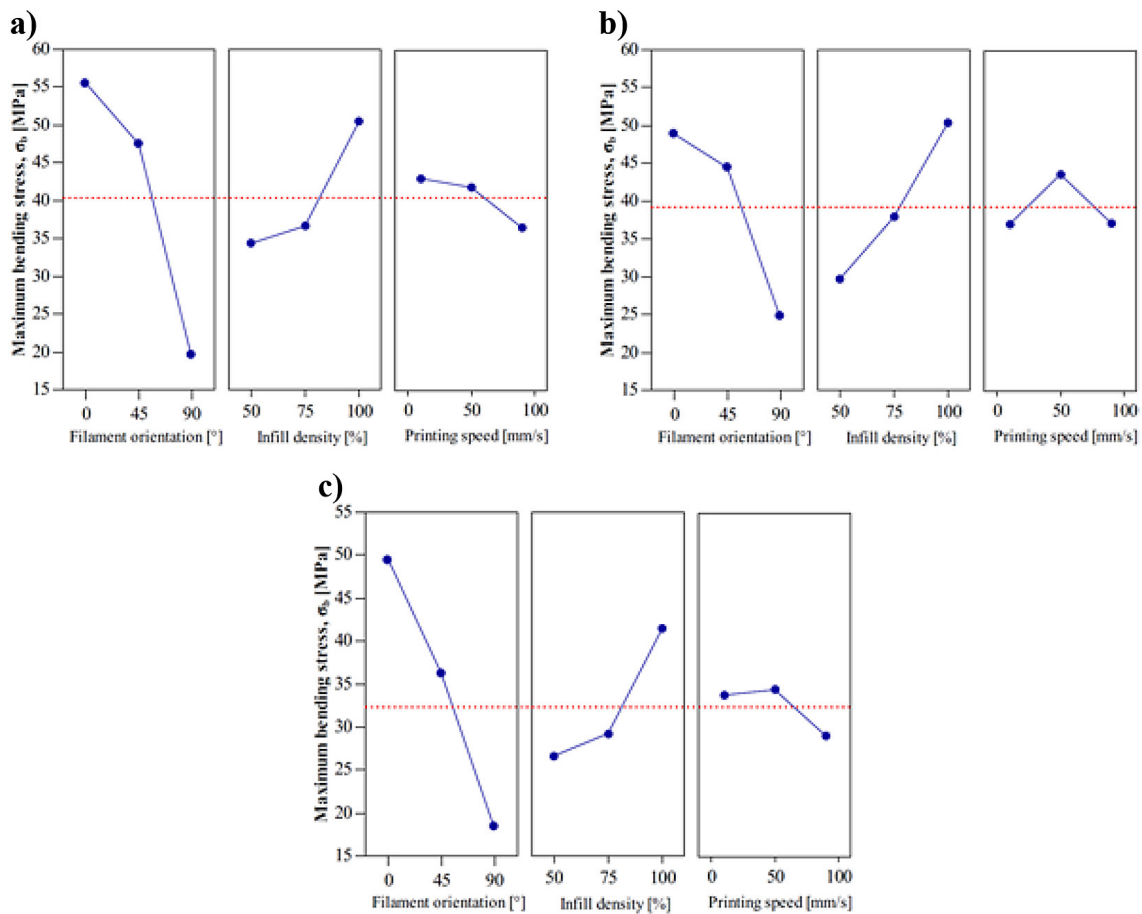

Figure 9. Main effects plot for means of the maximum bending stress (σb) for: (a) PLA, (b) ABS (c) PETG materials
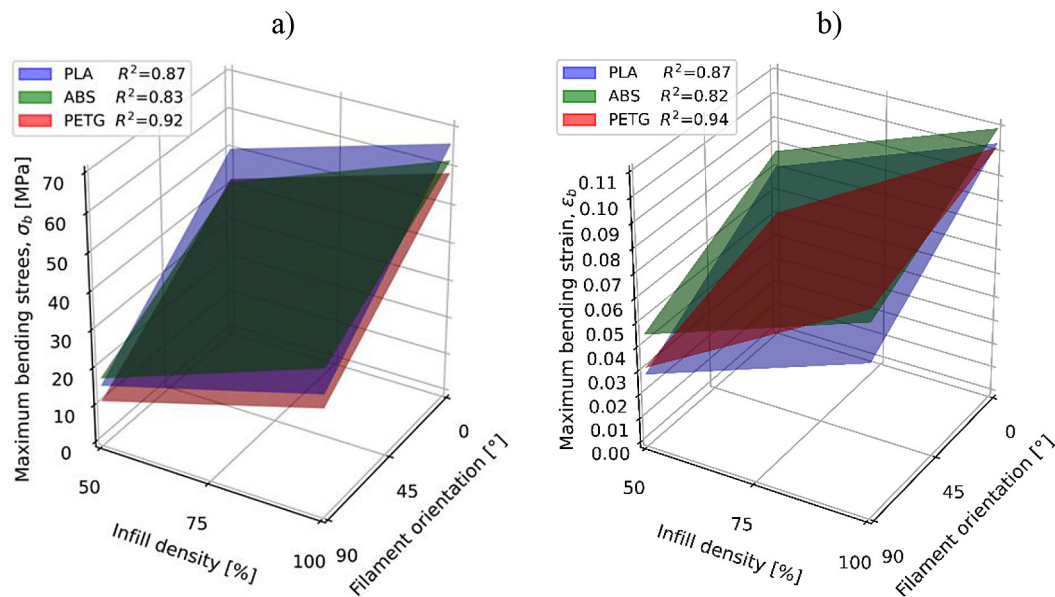
a)　　　　　　　　　　　　b)

Figure 10. Surface plots for the mechanical properties of the bending tests for PLA, ABS and PETG materials, (a) maximum bending stress (σb) and (b) maximum bending strain (εb).

CONCLUSIONS

The uniaxial tension and four point-bending samples manufactured with PLA, ABS, and PET materials under ASTM standards were evaluated. The effect of three parameters, *i.e.,* infill orientations, infill density, and printing speed defined by a design of experiments (DoE), was analyzed. The experimental findings lead to the following conclusions:

- In the three materials, the infill orientation is the most influential parameter in tensile strength, maximum deformation, and flexural resistance.
- PETG exhibited superior strength compared to PLA and ABS. This is related to the enhanced interlayer bonding. Also, PETG T1 exhibit the larger strain of all the samples with $\varepsilon_{u=0.040}$.
- Printing speed had a small effect on mechanical performance. This suggests that higher printing speeds can be utilized to optimize processing time and reduce manufacturing costs, without affecting mechanical performance.

Acknowledgments

REFERENCES

1. Wong KV, Hernández A. A review of additive manufacturing. ISRN Mech Eng. 2012;2012:1–10. doi:10.5402/2012/208760

2. Tofail SAM, Koumoulos EP, Bandyopadhyay A, Bose S, O'Donoghue L, Charitidis C. Additive manufacturing: scientific and technological challenges, market uptake and opportunities. Mater Today. 2018;21:22–37. https://doi.org/10.1016/j.mattod.2017.07.001

3. De Leon AC, Chen Q, Palaganas NB, Palaganas JO, Manapat J, Advincula RC. High-performance polymer nanocomposites for additive manufacturing applications. React Funct Polym. 2016;103:141–155. https://doi.org/10.1016/j.reactfunctpolym.2016.04.010

4. Schmitt M, Mehta RM, Kim IY. Additive manufacturing infill optimization for automotive 3D-printed ABS components. Rapid Prototyp J. 2020;26:89–99. https://doi.org/10.1108/RPJ-01-2019-0007

5. Barbosa WS, Gioia MM, Temporão GP, Meggiolaro MA, Gouvea FC. Impact of multi-lattice inner structures on FDM PLA 3D-printed orthosis using Industry 4.0 concepts. Int J Interact Des Manuf. 2022;17(1):371–383. https://doi.org/10.1007/s12008-022-00962-6

6. Górski F, Wichniarek R, Kuczko W, Żukowska M, Lulkiewicz M, Zawadzki P. Experimental studies on 3D printing of automatically designed customized wrist-hand orthoses. Materials (Basel). 2020;13(18):4091. https://doi.org/10.3390/ma13184091

7. Carneiro OS, Silva AF, Gomes R. Fused deposition modeling with polypropylene. Mater Des. 2015;83:768–776. https://doi.org/10.1016/j.matdes.2015.06.053

8. Cojocaru V, Frunzaverde D, Micloşină CO, Mărginean G. Influence of process parameters on the mechanical properties of PLA specimens produced by fused filament fabrication—a review. Polymers. 2022;14(5):886. https://doi.org/10.3390/polym14050886

9. Akhoundi B, Behravesh AH. Effect of filling pattern on the tensile and flexural mechanical properties of FDM 3D-printed products. Exp Mech. 2019;59:883–897. https://doi.org/10.1007/s11340-018-00467-y

10. Travieso-Rodriguez JA, Jerez-Mesa R, Llumà J, Traver-Ramos O, Gomez-Gras G, Roa Rovira JJ. Mechanical properties of 3D-printing polylactic acid parts subjected to bending stress and fatigue testing. Materials (Basel). 2019;12(23):3859. https://doi.org/10.3390/ma12233859

11. Cantrell JT, et al. Experimental characterization of the mechanical properties of 3D-printed ABS and polycarbonate parts. Rapid Prototyp J. 2017;23(4):811–824. doi:10.1108/RPJ-03-2016-0042

12. Samykano M, Selvamani SK, Kadirgama K, Ngui WK, Kanagaraj G, Sudhakar K. Mechanical property of FDM-printed ABS: influence of printing parameters. Int J Adv Manuf Technol. 2019;102(9–12):2779–2796. https://doi.org/10.1007/s00170-019-03313-0

13. Sepahi MT, Abusalma H, Jovanović V, Eisazadeh H. Mechanical properties of 3D-printed parts made of polyethylene terephthalate glycol. J Mater Eng Perform. 2021;30(11):6851–6861. https://doi.org/10.1007/s11665-021-06032-4

14. Khan SF, Zakaria H, Chong YL, Saad MAM, Basaruddin K. Effect of infill on tensile and flexural strength of 3D-printed PLA parts. In: IOP Conf Ser: Mater Sci Eng. 2018;429(1):012101. https://doi.org/10.1088/1757-899X/429/1/012101

15. Shubham P, Sikidar A, Chand T. Influence of layer thickness on mechanical properties of 3D-printed ABS polymer by fused deposition modeling. Key Eng Mater. 2016;706:63–67. https://doi.org/10.4028/www.scientific.net/KEM.706.63

16. Valvez S, Silva AP, Reis PNB. Optimization of printing parameters to maximize the mechanical properties of 3D-printed PETG-based parts. Polymers (Basel). 2022;14(13):2564. https://doi.org/10.3390/polym14132564

17. Torrado AR, Shemelya CM, English JD, Lin Y, Wicker RB, Roberson DA. Characterizing the effect of additives to ABS on mechanical property anisotropy of specimens fabricated by material-extrusion 3D printing. Addit Manuf. 2015;6:16–29. doi:10.1016/j.addma.2015.02.001

18. Tümer EH, Erbil HY. Extrusion-based 3D-printing applications of PLA composites: a review. Coatings. 2021;11(4):390. https://doi.org/10.3390/coatings11040390

19. Castro-Aguirre E, Iñiguez-Franco F, Samsudin H, Fang X, Auras R. Poly(lactic acid)—mass production, processing, industrial applications and end of life. Adv Drug Deliv Rev. 2016;107:333–366. https://doi.org/10.1016/j.addr.2016.03.010

20. Franco-Urquiza EA, Escamilla YR, Itzel P, Llanas A. Characterization of 3D printing on jute fabrics. Polymers. 2021;13(19):3202. doi:10.3390/polym13193202

21. Hong JH, Yu T, Chen Z, Park SJ, Kim YH. Improvement of flexural and compressive strength by heat treatment of PLA filament for 3D printing. Mod Phys Lett B. 2019;33(14–15):1940025. https://doi.org/10.1142/S0217984919400256

22. Chalgham A, Ehrmann A, Wickenkamp I. Mechanical properties of FDM-printed PLA parts before and after thermal treatment. Polymers. 2021;13(8):1239. doi:10.3390/polym13081239

23. Bhandari S, López-Anido RA, Gardner DJ. Enhancing the interlayer tensile strength of 3D-printed short carbon-fibre-reinforced PETG and PLA composites via annealing. Addit Manuf. 2019;30:100922. https://doi.org/10.1016/j.addma.2019.100922

24. Amza CG, Zapciu A, Constantin G, Baciu F, Vasile MI. Enhancing mechanical properties of polymer 3D-printed parts. Polymers. 2021;13(4):562. https://doi.org/10.3390/polym13040562

25. Chen L, Zhang X, Wang Y, Osswald TA. Laser polishing of Cu/PLA composite parts fabricated by fused deposition modeling: analysis of surface finish and mechanical properties. Polym Compos. 2020;41(4):1356–1368. https://doi.org/10.1002/pc.25459

26. Rahmatabadi D, Ghasemi I, Baniassadi M, Abrinia K, Baghani M. 3D printing of PLA–TPU with different component ratios: fracture toughness, mechanical properties and morphology. J Mater Res Technol. 2022;21:3970–3981. https://doi.org/10.1016/j.jmrt.2022.11.024

27. Chueca de Bruijn A, Gómez-Gras G, Pérez MA. Effect of ball burnishing on surface finish and mechanical performance of fused-filament-fabricated parts. Addit Manuf. 2021;46:102133. https://doi.org/10.1016/j.addma.2021.102133

28. Perera YS, Exley O, Dananjaya SAV, Hansika N, Abeykoon C. Investigation of the mechanical properties of 3D-printed hollow parts with finite element analysis. J Mater Res Technol. 2025;36:8826–8839. https://doi.org/10.1016/j.jmrt.2025.05.104

29. Abbot DW, Kallon DVV, Anghel C, Dube P. Finite element analysis of 3D printed model via compression tests. Procedia Manuf. 2019;35:164–173.

https://doi.org/10.1016/j.promfg.2019.06.001

30. Alarifi IM. Mechanical properties and numerical simulation of FDM 3D printed PETG/carbon composite unit structures. J Mater Res Technol. 2023;23:656–669. https://doi.org/10.1016/j.jmrt.2023.01.043

31. Alharbi M, Kong I, Patel VI. Simulation of uniaxial stress–strain response of 3D-printed polylactic acid by nonlinear finite element analysis. Appl Adhes Sci. 2020;8:5. https://doi.org/10.1186/s40563-020-00128-1

32. Sabik A, Rucka M, Andrzejewska A, Wojtczak E. Tensile failure study of 3D-printed PLA using DIC technique and FEM analysis. Mech Mater. 2022;175:104506. https://doi.org/10.1016/j.mechmat.2022.104506

33. Provaggi E, Capelli C, Rahmani B, Burriesci G, Kalaskar DM. 3D printing assisted finite element analysis for optimising the manufacturing parameters of a lumbar fusion cage. Mater Des. 2019;163:107540. https://doi.org/10.1016/j.matdes.2018.107540

34. Taregh M, Abusalama H, Jovanovic V, Eisazadeh H. Mechanical properties of 3D-printed parts made of polyethylene terephthalate. J Mater Eng Perform. 2021;30(11):6851–6861. https://doi.org/10.1007/s11665-021-06032-4

35. Levenhagen NP, Dadmun MD. Interlayer diffusion of surface segregating additives to improve the isotropy of fused deposition modeling products. Polymer. 2018;152:35–41. https://doi.org/10.1016/j.polymer.2018.01.031